

An optical nanofiber–based interface for single molecules

Sarah M. Skoff, David Papencordt, Hardy Schauffert, and Arno Rauschenbeutel
*Vienna Center for Quantum Science and Technology, Institute of Atomic and Subatomic Physics,
Vienna University of Technology, Stadionallee 2, 1020 Vienna, Austria*

Optical interfaces for quantum emitters are a prerequisite for implementing quantum networks. Here, we couple single molecules to the guided modes of an optical nanofiber. The molecules are embedded within a crystal that provides photostability and due to its inhomogeneous environment, a means to spectrally address single molecules. Single molecules are excited and detected solely via the nanofiber interface without the requirement of additional optical access. In this way, we realize a fully fiber-integrated system that is scalable and may become a versatile constituent for quantum hybrid systems.

In recent years, single molecules in solids [1–7] and other solid state quantum emitters such as NV centers and quantum dots have gained increased interest as building blocks for quantum networks [8, 9], quantum metrology [10] and nanosensors [11–13]. For all these applications, strong light–matter interactions are essential.

Strong light-matter interactions are either achieved by coupling to a large ensemble of quantum emitters [14, 15], employing a cavity [16] or decreasing the mode area of the interacting light field [17–20] and hence achieving a significant overlap between the absorption cross-section of the emitter and the respective light field. A versatile platform to achieve such a small effective mode area of the light field are optical nanofibers [20, 21]. An optical nanofiber is the waist of a tapered optical fiber (TOF) which has a diameter smaller than the wavelength of the light it is guiding. Therefore, an appreciable fraction of the light propagates outside the fiber in the form of an evanescent wave. Due to the strong transverse confinement of the light field, which prevails over the entire length of the nanofiber, the interaction with emitters close to the surface can be significant [19, 22–25].

Single molecules in crystalline solids are efficient quantum emitters that exhibit strong zero phonon lines (ZPL) which at cryogenic temperatures, can be as narrow as tens of MHz [26, 27]. Due to inhomogeneous broadening caused by the host crystal such molecules can be spectrally distinguished and individually addressed using a narrowband laser [28]. For a low doping of the crystal with molecules, this makes it possible to circumvent the additional spatial selection that has been used for numerous single molecule experiments in the past [29, 30], even if a large fraction of the crystal is illuminated. This was also exploited in a recent experiment by Faez et al. [17], where single dibenzoterrylene (DBT) molecules have been coupled to the modes of a nanocapillary.

Here, we show for the first time that single organic molecules can be interfaced with an optical nanofiber. This presents a new platform based on solid state emitters that can be used for quantum optics and is naturally integrated into any optical fiber network.

A TOF inside a cryostat (figure 1a) serves to optically

interface organic molecules, in our case terrylene in a para-terphenyl (p-terphenyl) crystal, with the evanescent light field surrounding its nanofiber. The nanofiber section has a total length of 3 mm and a diameter of 320 nm. The TOF is produced in a heat and pull process using a custom-made pulling rig [31]. In the 6.8 cm long tapered section of the fiber, the weakly guided LP₀₁ mode of the standard single mode optical fiber is adiabatically transformed into the strongly guided HE₁₁ mode of the nanofiber waist and back yielding minimal transmission losses of less than 2%. For our purpose, a broadband transmission is crucial as the excitation and detection wavelengths can differ by more than 100 nm. This requires a careful choice of tapering angles and waist diameter, details of which are reported in [32]. Terrylene in p-terphenyl exhibits four different electronic transitions from the ground to the first excited state termed X1–X4, corresponding to four possible orientations of these molecules in a p-terphenyl crystal. Terrylene molecules in the X4 orientation are resonant with light at 577.9 nm and have been shown to be very stable [33]. Hence, all measurements presented here use molecules in this site. A simplified level diagram is depicted in figure 1b. The laser excites the molecule on the 00ZPL, the zero phonon line that connects the ground and the excited electronic state without any vibrational contribution of the molecule. After excitation, the molecule will decay into any of the vibrational states in the electronic ground state with a probability determined by the Franck Condon and Debye-Waller factors. From these states it will nonradiatively decay into the vibrational ground state within ps. Hence the absorption cross-section [34] of a single molecule in a solid is

$$\sigma = \frac{3\lambda^2}{2\pi} \frac{\Gamma^2}{\Gamma_{\text{hom}}^2} \frac{(\mathbf{e} \cdot \mathbf{d})^2}{|\mathbf{d}|^2} \quad (1)$$

where the product $\mathbf{e} \cdot \mathbf{d}$ represents the projection of the polarisation vector \mathbf{e} of the excitation light on the molecular dipole \mathbf{d} and λ denotes the excitation wavelength. Γ is the lifetime limited linewidth and Γ_{hom} the homogeneously broadened linewidth of the molecule, respectively. If the dipole is aligned with the polarisation of the

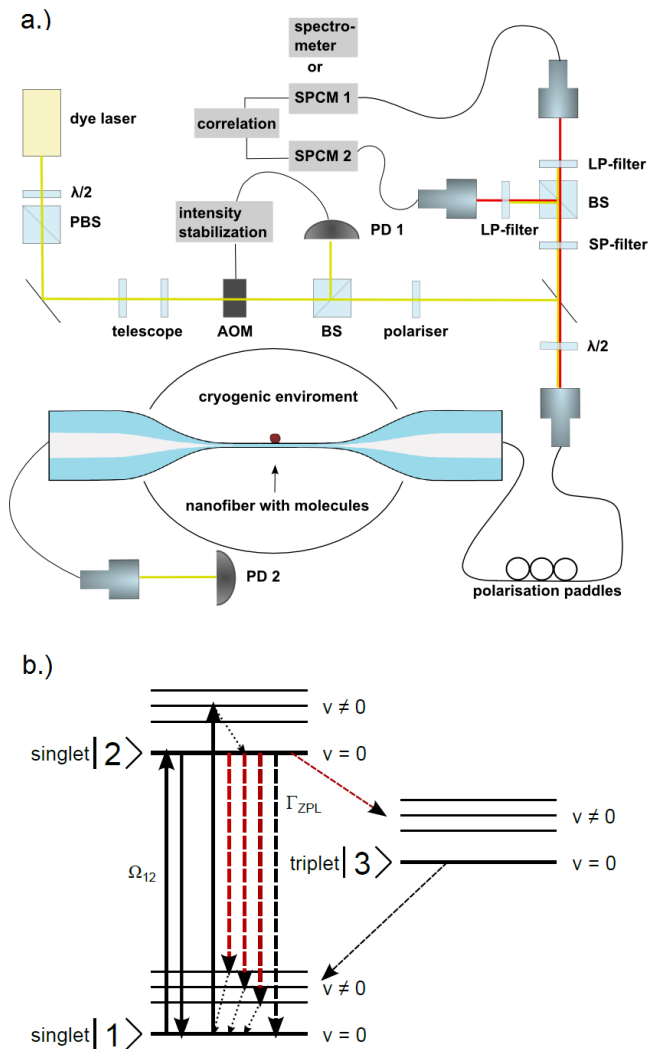


Figure 1. a.) Experimental set-up for single molecule spectroscopy via an optical nanofiber interface. b.) Simplified level diagram of terrylene in p-terphenyl. Full lines indicate transitions driven by the laser, while dashed lines represent spontaneous emission. Dotted lines within an electronic manifold correspond to non-radiative decay processes that occur on a timescale of ps.

incident light and the homogeneous broadening is negligible, the absorption cross-section will be that of a simple two-level atom and is comparable to the effective mode area [35] of our optical nanofiber which is $0.5 \times \lambda^2$. This ensures a strong effect of a single molecule on the light field. The probability of a terrylene molecule to decay to the triplet state after excitation instead of the singlet ground state is very low and has experimentally been found to be $< 10^{-5}$ at cryogenic temperatures [2, 36]. To maintain sufficient light guiding capabilities of the nanofiber-crystal system for spectroscopy and to ensure

that the crystal stays tightly adhered to the vertically mounted nanofiber, the crystals have to be on the order of a few hundred nanometers in size. Such nanocrystals are grown by a reprecipitation method [37] from an oversaturated solution of a 8×10^{-5} molar mixture of terrylene/p-terphenyl in toluene. The solution is heated until both compounds are dissolved and then isopropanol is added as a reprecipitation agent. This procedure results in terrylene doped p-terphenyl crystals of platelet morphology as seen in figure 2a, which shows a scanning electron microscope (SEM) image of such crystals deposited on a silicon substrate. The majority of crystals have base dimensions in the range of 200 to 2000 nm and a base width to height ratio of 2.5:1 to 5:1 as determined by atomic force microscopy (AFM) measurements. The monocrystalline nature of these crystals has been verified by performing selected area electron diffraction (SAED) measurements using a transmission electron microscope (TEM), see figure 2b. SAED also indicates that the substrate supported crystal platelet base face is of (001) orientation, i.e. the crystal's c-axis is perpendicular to the substrate. It is known that the dipole moment of the lowest electronically excited state in terrylene lies along the long axis of the molecule [33]. When inserted into a p-terphenyl crystal, the molecule's long axis and thus the dipole moment lie nearly parallel to the crystal's c-axis and therefore roughly perpendicular to the substrate.

A terrylene doped p-terphenyl nanocrystal is deposited on the nanofiber by a drop-touch method: a drop of the suspension containing doped p-terphenyl nanocrystals is briefly brought into contact with the nanofiber via a pipette. During this process the transmission and fluorescence of the nanofiber is monitored with a power meter and a spectrometer, respectively. When a doped crystal has adhered to the nanofiber surface during the brief contact with the suspension droplet, a typical fluorescence signal and some loss in transmission is observed. As crystals of a variety of sizes are produced during our growth process we can only post-select the size of the deposited crystals. However since the largest crystals sediment faster, we usually find a suitable small one in the suspension supernatant. If it is nevertheless found that the transmission deteriorates too much during the deposition process, the crystal can be washed off with acetone and another one will be deposited.

The TOF with the crystal is mounted on a steel holder with two NdFeB magnets that ensure the fiber is firmly held and that it stays intact during the cooling process down to cryogenic temperatures. This fiber set-up is mounted in the cold pot of a custom-made cryostat that can cool the sample to 4 K. To ensure efficient thermalisation of the nanofiber and the crystal with the walls of the cold pot, helium buffer gas at a pressure of a few mbar is introduced into the cold pot, after it has been evacuated before cool-down. The temperature of the cryostat cold pot is measured by a Cernox silicon diode tempera-

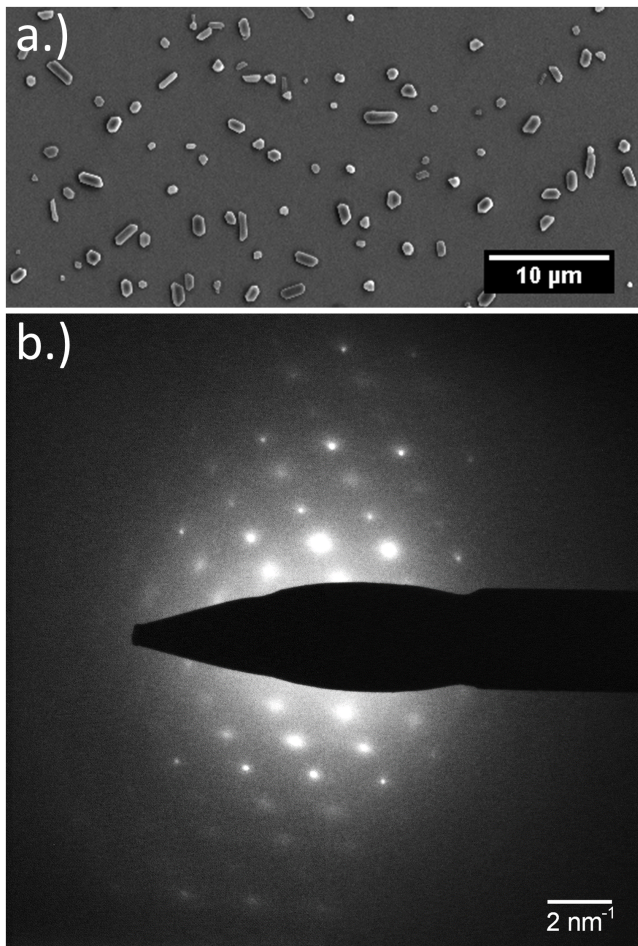


Figure 2. a.) Scanning electron microscope image (FEI Quanta 200 FEG) of terrylene doped p-terphenyl crystals on a silicon substrate. b.) Selected area electron diffraction (SAED) pattern of an individual terrylene-doped paraterphenyl crystal (Philips CM200 TEM at 200 kV, imaged with the electron beam perpendicular to the crystal base face, exposure time was kept short (≤ 3 s) to avoid electron beam induced degradation of the organic crystal [38]). The pattern is consistent with the monoclinic high-temperature phase of a single para-terphenyl crystal [39] viewed along the [001] axis (considering double diffraction effects, Cambridge Structural Database (CSD) entry terphe14).

ture sensor.

To excite the molecules, light of a dye laser is coupled into the optical fiber that connects to the TOF and that enters the cryostat via a teflon feed-through (figure 1a). To compensate for fast intensity fluctuations of the excitation light down to a bandwidth of 1 Hz, the laser beam is sent through an acousto-optic modulator and is actively intensity stabilised. A fraction of the Stokes-shifted fluorescence of the molecule is collected by the nanofiber, fiber-guided out of the cryostat, and monitored by a spectrometer (Shamrock SR-303i, Andor Technology) or single photon counting modules

(SPCMs). Contributions from the excitation light and fluorescence on the 00ZPL are filtered out by a long-pass filter. Together with a short-pass filter to block Raman scattering from the fiber, this leaves a transmission window of 630-650 nm.

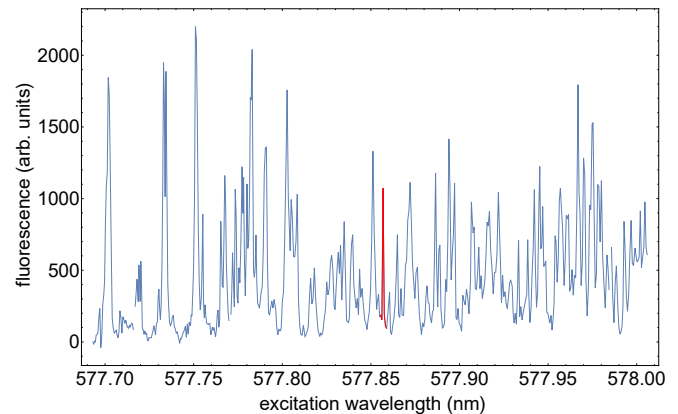


Figure 3. Fluorescence excitation measurement of nanofiber-interfaced terrylene molecules. The red peak indicates the fluorescence of a single terrylene molecule.

Due to the inhomogeneous line shifts induced by the host crystal matrix, single molecules can be spectrally selected with the narrowband dye laser if the terrylene concentration in the host crystal is dilute enough. Figure 3 shows the fluorescence excitation spectrum of a molecular ensemble in the X4 orientation. The excitation line of a verified single molecule is highlighted in red.

To test the optical interface created by individual molecules and the optical nanofiber, we have investigated four different single molecules. To verify the interaction with single quantum emitters, second order fluorescence intensity correlation measurements are performed. A Hanbury-Brown-Twiss (HBT) set-up is used (figure 1a), where the backscattered fluorescence is split by a 50/50 beamsplitter and directed to two SPCMs. The counts are recorded by means of a field programmable gate array (FPGA) and then correlated. For a single quantum emitter, photon antibunching is observed, which manifests itself as an antibunching dip in the intensity correlation measurements at zero time delay τ between two detection events. Experimental imperfections such as incoherent background scatter will reduce the contrast of the dip but a dip deeper than 50% of the coincidence rates at long correlation times is proof of a single quantum emitter. Figure 4 shows second order fluorescence intensity correlation measurements of a molecule on the nanofiber where the antibunching dip is clearly visible. As the excitation intensity is increased, the onset of Rabi oscillations is apparent. Since the decay into the triplet state is negligible for short times, the measurements are fitted to the correlation function that is obtained by solving the Bloch equations for a two level system with a spontaneous de-

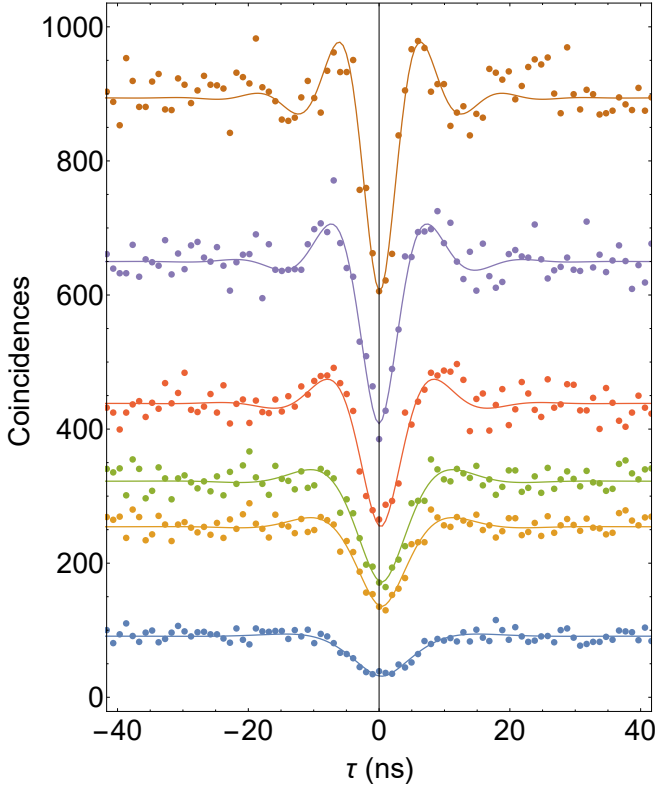


Figure 4. Fluorescence intensity correlation measurements of molecule B for different excitation powers. The coincidences were recorded over a period of 1000 s and the time resolution for the data is 1 ns. With increasing excitation power the onset of Rabi oscillations and an increase in incoherent background scatter is clearly seen.

cay rate Γ and a Rabi frequency $\Omega = \mathbf{E} \cdot \mathbf{d}/\hbar$, where \mathbf{d} is the dipole moment of the molecule and \mathbf{E} the electric field at the molecule's location [34].

$$g^2(\tau) = 1 - \left[\cos(\nu\tau) + \frac{3\Gamma}{4\nu} \sin(\nu\tau) \right] \exp\left(\frac{-3\Gamma\tau}{4}\right)$$

with

$$\nu = \sqrt{\Omega^2 - \left(\frac{\Gamma}{4}\right)^2}$$

Fitting eqn.(2) to the data for different excitation powers while using Γ as a global fit parameter for all measurements on a given molecule, yields the respective Rabi frequencies and the non-power broadened homogeneous linewidth Γ of the molecule. From these fits we can obtain the saturation intensity I_S of the molecule as $\frac{I}{I_S} = \frac{2\Omega^2}{\Gamma^2}$. Figure 5 shows this expected linear increase of the squared Rabi frequency as a function of excitation power for three different molecules in the same crystal. The errorbars obtained from fitting the intensity correlation measurements are smaller than the depicted datapoints in figure 5. From the fits the saturation power P_S , corresponding to I_S is obtained. We convert P_S to the maximum intensity at the surface of

the nanofiber. Without the exact knowledge of the orientation of the molecule's transition dipole moment and its distance from the nanofiber surface, this gives an upper limit for the saturation intensity. In this way we obtain saturation powers for molecule A of $P_S = 1.8 \pm 0.3$ nW, molecule B of $P_S = 4.3 \pm 0.8$ nW and molecule C of $P_S = 0.5 \pm 0.1$ nW, which corresponds to saturation intensities of $I_S < 1.8 \text{ Wcm}^{-2}$, $I_S < 4.3 \text{ Wcm}^{-2}$ and $I_S < 0.5 \text{ Wcm}^{-2}$, respectively. The biggest error in the saturation powers arises due to the uncertainty in determining the power in the fiber which is reflected by the error given for the final result. For the saturation intensities this error is insignificant compared to the uncertainty that stems from the unknown distance from the nanofiber surface and the overlap of the polarisation vector of the light field and the molecule's dipole moment. Therefore, only an upper limit is stated. The obtained saturation intensities are similar to results obtained by other groups who studied terrylene in bulk p-terphenyl [26, 40]. To our knowledge a saturation intensity of $I_S < 0.5 \text{ Wcm}^{-2}$ as for molecule C is the lowest measured so far for terrylene in p-terphenyl. As opposed to measurements on terrylene in bulk p-terphenyl using a confocal microscope, the excitation light in our case enters through the side of the thin host crystal platelets. As the transition dipole moment of the molecules lies nearly perpendicular to the base of these platelets, this suggests an improved overlap between the polarisation of the nanofiber guided excitation light and the transition dipole moment of the molecules. An independent measurement of the satura-

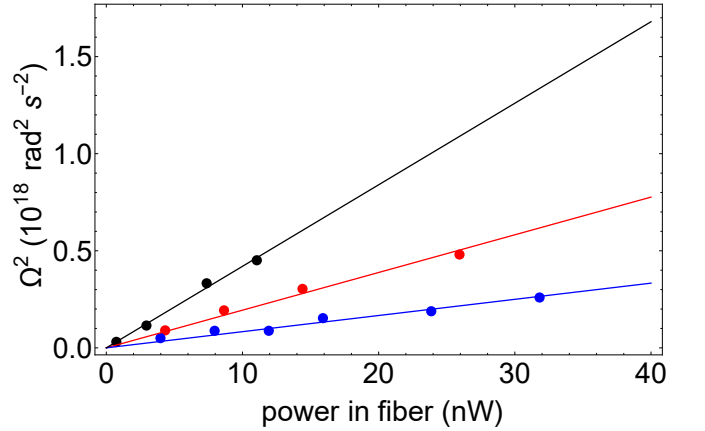


Figure 5. Squared Rabi frequency as a function of in fiber power for molecule A (red), B (blue) and C (black).

tion power is obtained by recording the fluorescence rate R on resonance as a function of excitation power as seen in figure 6, which includes a fit to $R = R_\infty \frac{P/P_S}{1+P/P_S}$. The errorbars on the fluorescence rate that are obtained by taking the standard error of the amplitude from fits over several molecular spectra are smaller than the depicted datapoints. This measurement yields a saturation power of 4.8 ± 1.4 nW for molecule B, where the error comes

from the fit and the uncertainty in the excitation power inside the fiber. Analogous to above this translates into a saturation intensity of $I_S < 4.8 \text{ Wcm}^{-2}$ for molecule B in good agreement with $I_S < 4.3 \text{ Wcm}^{-2}$ as obtained with the HBT setup. We performed a further measure-

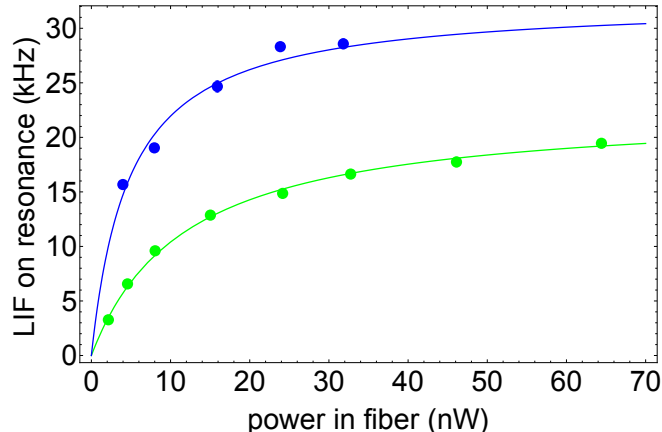


Figure 6. Saturation of the resonant fluorescence intensity as the excitation laser power is increased for molecules B (blue) and D (green).

ment on a molecule (molecule D) that was found to show lower fluorescence rates and indeed was measured to have a higher saturation power of $11.4 \pm 2.2 \text{ nW}$ and therefore a saturation intensity of $< 11.4 \text{ Wcm}^{-2}$. This suggests that it is located further from the nanofiber surface such that fluorescence does not couple back to the nanofiber interface as efficiently. Alternatively, the alignment between polarisation of the excitation beam and the molecular dipole moment of molecule D may be less favorable. Although all molecules are embedded in a single crystal and therefore have the same orientation, the inherent birefringence of the host crystal can cause such a less favorable alignment, as the induced phase shift on the propagating light field is $\Delta\phi = 2\pi\Delta nL/\lambda$, where λ is the vacuum wavelength, L the propagation distance and Δn is the effective birefringence that can be up to 0.32 in our case. The overall efficiency for fluorescence excitation and detection via the nanofiber interface is given as $\eta_{\text{LIF}} \propto |\mathbf{d} \cdot \mathbf{E}|^2 \beta$, where $\beta = \frac{\Gamma_g}{\Gamma_{sc}}$ is the coupling efficiency of dipole radiation to the nanofiber modes. This coupling efficiency is dependent on the distance and its orientation with respect to the nanofiber surface. Γ_g is the scattering rate into guided modes and Γ_{sc} is the total scattering rate of the dipole. For our case, using a nanofiber of 160 nm radius and Stokes shifted fluorescence in the range of 630 – 650 nm this coupling efficiency for a radially, azimuthally and axially oriented dipole has been calculated following [22] and is depicted in figure 7. Since the saturation intensity measured for molecule C is the lowest yet measured for terrylene in p-terphenyl, it is assumed to be very close to the surface of the nanofiber. The maximum distance of the other

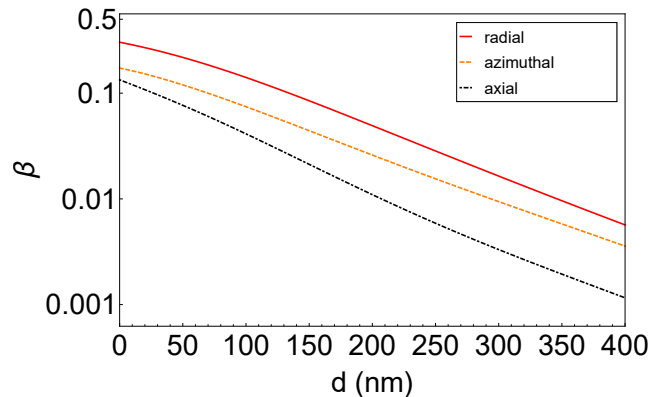


Figure 7. Mean coupling efficiency of a linear radial (red), tangential (orange, dashed) and axial (black, dot dashed) dipole, radiating at 630-650 nm, to the nanofiber as a function of distance from the nanofiber surface.

molecules from the nanofiber surface can then be estimated by comparing their saturation intensities. As we did not actively align the polarisation before each measurement on a new molecule to achieve maximum overlap between polarisation of the light and the molecule's transition dipole moment and because the host crystal is birefringent, we can only give an upper limit on the radial distance between the different molecules. To illustrate this more clearly, figure 8 shows the efficiency of fluorescence excitation and detection via the nanofiber interface for different positions of the dipole with respect to the nanofiber surface. The positions are chosen to be consistent with the volume of a platelet crystal that is lying with its base on the nanofiber surface. The molecular dipole is oriented perpendicular to the crystal's base and excited by quasilinear light via the nanofiber-based interface. Incorporating the refractive index of the crystal into this model would make the local efficiencies very dependent on the crystal's geometry and as we are only interested in assigning the maximum radial distance of the measured molecules, we have neglected the refractive index of the crystal at this point. The maximum radial distances of the investigated molecules are depicted in their respective colours by dashed contours (fig. 8) and these results show that radially they all lie within less than 280 nm of each other and less than 160 nm from the nanofiber surface, which is consistent with high coupling efficiencies of the molecules to the guided nanofiber modes (fig. 7).

Summarizing, we have successfully shown how single molecules can be optically interfaced via the evanescent field surrounding an optical nanofiber. This is an important addition to the toolbox of quantum emitters such as atoms [20, 41, 42], quantum dots [19, 43] and NV centers in nanodiamonds [25, 44] that have been fully fiber-integrated by coupling to optical nanofibers. Each of these systems has its own intrinsic advantages

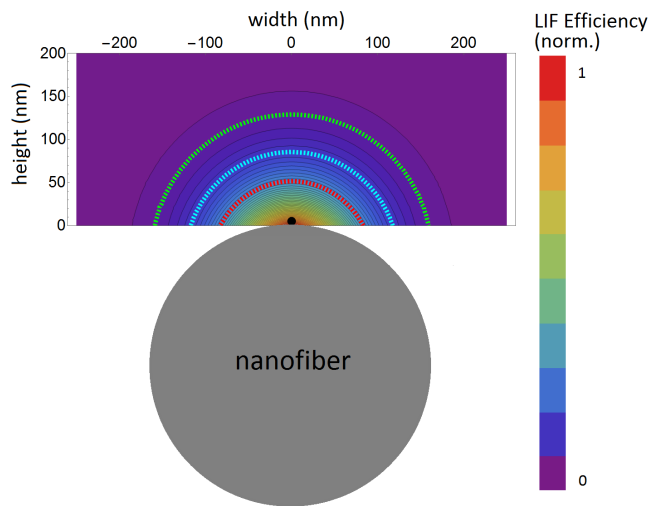


Figure 8. The fluorescence efficiency for a molecular dipole at different positions with respect to the nanofiber. The spatial coordinates are chosen assuming a platelet crystal that is lying with its base on the nanofiber surface. The contact point of nanofiber and crystal is at the origin of this reference frame. The fluorescence efficiency is normalised to the maximum fluorescence efficiency on the nanofiber surface of 8% (excitation and detection). The maximum radial distances for the different molecules are indicated by dashed colored lines (A = red, B = blue, D = green). The reference molecule C is shown as a black dot and is assumed to be located directly on the nanofiber surface at position $(x,y) = (0,0)$.

and usage for quantum networks. Single molecules in solids are efficient quantum emitters over a broad range of wavelengths, which makes them suitable to be interfaced with other quantum emitters [1]. They have an advantageous level structure for the implementation of triggered single photon sources [27, 45] and have shown their versatility in quantum optics [46–48]. Further, single molecules coupled to waveguides allow the investigation of photon-mediated interactions between two quantum emitters even when they are separated by more than the excitation wavelength [49–51]. These interactions can be further enhanced by using a nanofiber between two fiber Bragg gratings which makes a high Q-cavity [52]. Single molecules interacting with the evanescently guided light field of optical nanofibers therefore not only offer a rich experimental platform for investigating entanglement and correlations between quantum emitters but also provide a means for implementing components of any quantum networks such as fibre coupled single photon sources [18, 53, 54] or photon sorters [55].

ACKNOWLEDGMENTS

The authors thank Dr. Bernhard C. Bayer (University of Vienna, Austria) for SAED and AFM measurements on

the terrylene doped p-terphenyl crystals. This work was supported by the Federal Ministry of Science, Research and Economy of Austria.

-
- [1] P. Siyushev, G. Stein, J. Wrachtrup, and I. Gerhardt, *Nature* **509**, 66 (2014).
 - [2] T. Basch, T., S. Kummer, and C. Braeuchle, *Nature* **373**, 132 (1995).
 - [3] T. Basch, W. E. Moerner, M. Orrit, and H. Talon, *Physical Review Letters* **69**, 1516 (1992).
 - [4] M. Celebrano, P. Kukura, A. Renn, and V. Sandoghdar, *Nature Photonics* **5**, 95 (2011).
 - [5] I. Gerhardt, G. Wrigge, P. Bushev, G. Zumofen, M. Agio, R. Pfab, and V. Sandoghdar, *Physical Review Letters* **98**, 033601 (2007).
 - [6] I. Gerhardt, G. Wrigge, J. Hwang, G. Zumofen, and V. Sandoghdar, *Phys. Rev. A* **82**, 063823 (2010).
 - [7] B. Kozankiewicz and M. Orrit, *Chemical Society Reviews* **43**, 1029 (2014).
 - [8] K. Nemoto, M. Trupke, S. J. Devitt, A. M. Stephens, B. Scharfenberger, K. Buczak, T. Nbauer, M. S. Everitt, J. Schmiedmayer, and W. J. Munro, *Physical Review X* **4**, 031022 (2014).
 - [9] G. Goldstein, P. Cappellaro, J. R. Maze, J. S. Hodges, L. Jiang, A. S. Sørensen, and M. D. Lukin, *Physical Review Letters* **106**, 140502 (2011).
 - [10] M. W. Doherty, V. V. Struzhkin, D. A. Simpson, L. P. McGuinness, Y. Meng, A. Stacey, T. J. Karle, R. J. Hemley, N. B. Manson, L. C. Hollenberg, and S. Praver, *Physical Review Letters* **112**, 047601 (2014).
 - [11] S. Faez, S. J. van der Molen, and M. Orrit, *Physical Review B* **90**, 205405 (2014).
 - [12] G. Mazzamuto, A. Tabani, S. Pazzagli, S. Rizvi, A. Reserbat-Plantey, K. Schdler, G. Navickaite, L. Gaudreau, F. S. Cataliotti, F. Koppens, and C. Toninelli, *New Journal of Physics* **16**, 113007 (2014).
 - [13] G. Kucsko, P. C. Maurer, N. Y. Yao, M. Kubo, H. J. Noh, P. K. Lo, H. Park, and M. D. Lukin, *Nature* **500**, 54 (2013).
 - [14] M. D. Lukin and A. Imamoglu, *Nature* **413**, 273 (2001).
 - [15] K. F. Reim, J. Nunn, V. O. Lorenz, B. J. Sussman, K. C. Lee, N. K. Langford, D. Jaksch, and I. A. Walmsley, *Nature Photonics* **4**, 218 (2010).
 - [16] J. Volz, M. Scheucher, C. Junge, and A. Rauschenbeutel, *Nature Photonics* **8**, 965 (2014).
 - [17] S. Faez, P. Türschmann, H. R. Haakh, S. Götzinger, and V. Sandoghdar, *Physical Review Letters* **113**, 213601 (2014).
 - [18] J. Hwang and E. A. Hinds, *New Journal of Physics* **13**, 085009 (2011).
 - [19] R. Yalla, F. Le Kien, M. Morinaga, and K. Hakuta, *Phys. Rev. Lett.* **109**, 063602 (2012).
 - [20] E. Vetsch, D. Reitz, G. Sagu, R. Schmidt, S. T. Dawkins, and A. Rauschenbeutel, *Phys. Rev. Lett.* **104**, 203603 (2010).
 - [21] R. Garcia-Fernandez, W. Alt, F. Bruse, C. Dan, K. Karapetyan, O. Rehband, A. Stiebeiner, U. Wiedemann, D. Meschede, and A. Rauschenbeutel, *Applied Physics B* **105**, 3 (2011).

- [22] F. Le Kien, S. Dutta Gupta, V. I. Balykin, and K. Hakuta, *Physical Review A* **72**, 032509 (2005).
- [23] D. Reitz, C. Sayrin, R. Mitsch, P. Schneeweiss, and A. Rauschenbeutel, *Phys. Rev. Lett.* **110**, 243603 (2013).
- [24] K. P. Nayak, P. N. Melentiev, M. Morinaga, F. L. Kien, V. I. Balykin, and K. Hakuta, *Opt. Express* **15**, 5431 (2007).
- [25] L. Liebermeister, F. Petersen, A. v. Mnchow, D. Burchardt, J. Hermelbracht, T. Tashima, A. W. Schell, O. Benson, T. Meinhardt, A. Krueger, A. Stiebeiner, A. Rauschenbeutel, H. Weinfurter, and M. Weber, *Applied Physics Letters* **104**, 031101 (2014).
- [26] S. Kummer, T. Basch, and C. Bruchle, *Chemical Physics Letters* **229**, 309 (1994).
- [27] W. E. Moerner, *New Journal of Physics* **6**, 88 (2004).
- [28] W. E. Moerner and M. Orrit, *Science* **283**, 1670 (1999).
- [29] J. Michaelis, C. Hettich, A. Zayats, B. Eiermann, J. Mlynek, and V. Sandoghdar, *Optics Letters* **24**, 581 (1999).
- [30] P. Tamarat, A. Maali, B. Lounis, and M. Orrit, *The Journal of Physical Chemistry A* **104**, 1 (2000).
- [31] F. Warken, A. Rauschenbeutel, and T. Bartholomaus, *Photonics Spectra* **42**, 73 (2008).
- [32] A. Stiebeiner, R. Garcia-Fernandez, and A. Rauschenbeutel, *Opt. Express* **18**, 22677 (2010).
- [33] P. Bordat and R. Brown, *The Journal of Chemical Physics* **116**, 229 (2002).
- [34] R. Loudon, *The Quantum Theory of Light* (OUP Oxford, 2000).
- [35] F. Warken, E. Vetsch, D. Meschede, M. Sokolowski, and A. Rauschenbeutel, *Optics Express* **15**, 11952 (2007).
- [36] M. Banasiewicz, O. Morawski, D. Wicek, and B. Kozankiewicz, *Chemical Physics Letters* **414**, 374 (2005).
- [37] H. Kasai, H. S. Nalwa, H. Oikawa, S. Okada, H. Matsuda, N. Minami, A. Kakuta, K. Ono, A. Mukoh, and H. Nakanishi, *Japanese Journal of Applied Physics* **31**, L1132 (1992).
- [38] P. Li and R. F. Egerton, *Ultramicroscopy* **101**, 161 (2004).
- [39] A. P. Rice, F. S. Tham, and E. L. Chronister, *Journal of Chemical Crystallography* **43**, 14 (2012).
- [40] P. Tamarat, B. Lounis, J. Bernard, M. Orrit, S. Kummer, R. Kettner, S. Mais, and T. Basch, *Physical Review Letters* **75**, 1514 (1995).
- [41] A. Goban, K. S. Choi, D. J. Alton, D. Ding, C. Lacrote, M. Pototschnig, T. Thiele, N. P. Stern, and H. J. Kimble, *Phys. Rev. Lett.* **109**, 033603 (2012).
- [42] M. Hafezi, Z. Kim, S. L. Rolston, L. A. Orozco, B. L. Lev, and J. M. Taylor, *Physical Review A* **85**, 020302 (2012).
- [43] M. Fujiwara, K. Toubaru, T. Noda, H.-Q. Zhao, and S. Takeuchi, *Nano Letters* **11**, 4362 (2011).
- [44] M. Fujiwara, H.-Q. Zhao, T. Noda, K. Ikeda, H. Sumiya, and S. Takeuchi, *Optics Letters* **40**, 5702 (2015).
- [45] B. Lounis and W. E. Moerner, *Nature* **407**, 491 (2000).
- [46] J. Hwang, M. Pototschnig, R. Lettow, G. Zumofen, A. Renn, S. Gtzinger, and V. Sandoghdar, *Nature* **460**, 76 (2009).
- [47] M. Pototschnig, Y. Chassagneux, J. Hwang, G. Zumofen, A. Renn, and V. Sandoghdar, *Phys. Rev. Lett.* **107**, 063001 (2011).
- [48] A. Maser, B. Gmeiner, T. Utikal, S. Gtzinger, and V. Sandoghdar, arXiv:1509.05216 [physics, physics:quant-ph] (2015), arXiv: 1509.05216.
- [49] S. Rist, J. Eschner, M. Hennrich, and G. Morigi, *Physical Review A* **78**, 013808 (2008).
- [50] A. F. v. Loo, A. Fedorov, K. Lalumire, B. C. Sanders, A. Blais, and A. Wallraff, *Science* **342**, 1494 (2013).
- [51] F. Le Kien, S. D. Gupta, K. P. Nayak, and K. Hakuta, *Physical Review A* **72**, 063815 (2005).
- [52] C. Wuttke, M. Becker, S. Brckner, M. Rothhardt, and A. Rauschenbeutel, *Opt. Lett.* **37**, 1949 (2012).
- [53] V. Ahtee, R. Lettow, R. Pfab, A. Renn, E. Ikonen, a. S. Gtzinger, and V. Sandoghdar, *Journal of Modern Optics* **56**, 161 (2009).
- [54] C. Polisseni, K. D. Major, S. Boissier, S. Grandi, A. S. Clark, and E. A. Hinds, *Optics Express* **24**, 5615 (2016).
- [55] D. Witthaut, M. D. Lukin, and A. Sørensen, *EPL* **97**, 50007 (2012).